Breaking of Ketene Bonds during HCl Addition to Trimethylsilylketene

Nathalie Piétri,*,† Anouk Gaudel-Siri,*,‡ Isabelle Couturier-Tamburelli,† Jean-Marc Pons,‡ and Jean-Pierre Aycard†

Laboratoire PIIM-UMR 6633, Université de Provence, Centre Scientifique de St-Jérôme, Case 252, av. Esc. Normandie-Niemen, 13397 Marseille Cedex 20, France, and Laboratoire SymBio-UMR 6178, Université Paul Cézanne, Faculté des Sciences et Techniques, Case D12, av. Esc. Normandie-Niemen, 13397 Marseille Cedex 20, France

Received: November 9, 2004; In Final Form: January 3, 2005

IR spectroscopy is coupled with the matrix isolation technique to study the reaction of trimethylsilylketene with HCl. From 50 K trimethylsilylketene reacts with hydrogen chloride, leading to the cleavage of the Si−C bond and the formation of trimethylsilyl chloride and acetyl chloride, through intermediate trimethylsilylacetyl chloride which was identified. A reaction profile for this result is proposed based on a theoretical study carried out at the DFT level.

1. Introduction

Reactions between ketenes and electrophiles, as well as ketene−hydrogen halide complexes, have attracted the attention of many experimental and theoretical chemists.[1,2] Recent investigations on these complexes, generated in the gas or the solid phase, show a strong interaction between the hydrogen atom of the halide and the terminal carbon atom of the ketene moiety.[3] In this kind of reaction, interconversion of ketenes and acyl halides via acylium ions is a well-established process. However, some results seem indicative of the formation of unobserved enol intermediates.

Among the ketene family, silylketenes, discovered 40 years ago[4] are remarkably stable when compared to other ketenes; thus, trimethylsilylketene (**1**) has an extraordinary resistance toward dimerization and its low reactivity in hydration reactions (hydration of **1** is 400 times slower than the same reaction with tBuCH═C═O[5]) reflects the ground-state stability of this ketene. Despite their stability, silylketenes, which can be prepared through various ways, display a significant reactivity.[6] Like all ketenes, they can undergo nucleophilic attack but reagents must be rather strong or electrophilic activation (Lewis acid) is required; most applications deal with the formation of esters from alcohols. The other main type of reaction in which silylketenes can be successfully engaged is cycloaddition reactions, [2+2] and [4+2]. Natural products, including several β-lactones[7] and nitrogen-heterocycles,[6d] have been synthesized through this approach: for example, tetrahydrolipstatine[7a] and isoquinolides[8] were obtained in good yields from trimethylsilylketenes.

Experiments in the gas phase showed a reaction between **1** and HCl which involves a cleavage of the Si−C bond and the formation of trimethylsilyl chloride (**4**) and acetyl chloride (**5**; Scheme 1). The purpose of the present work is to monitor this reaction, from the initial formation of molecular van der Waals complexes, through transition states and unstable intermediates, to final products. Matrix isolation experiments were used to trap highly reactive intermediates and were monitored by FT-IR spectroscopy. Quantum calculations were undertaken to compare the experimental IR spectra with the calculated ones and thus assign observed absorptions, and furthermore, to determine the complex structures and the reaction path.

SCHEME 1 : Reaction of Formation of $SiMe_3Cl$ and MeCOCl

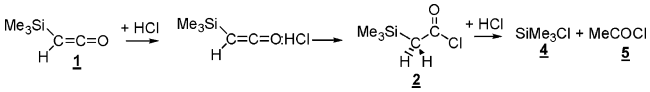

2. Experimental Section

Pure trimethylsilylketene (**1**) was prepared according to the original method,[4,6e] and trimethylsilylacetyl chloride **2** was synthesized as described in the literature.[9] Acetyl chloride and chlorotrimethylsilane were supplied by Aldrich and used without further purification.

2.1. Matrix Isolation Experiments. The gas mixtures of **1**/Ar and HCl/Ar were prepared by standard manometric techniques. We obtained relative concentration (**1**/HCl/Ar: 1/3/500, 1/10/500, 3/1/500, and 10/1/500) sprayed by co-deposition onto a gold-plated copper surface cooled to 20 K. A Fourier transform infrared spectrometer (Nicolet Serie II magma 750) was used to record the samples spectra cooled at 10 K by reflectance in the range 4000−550 cm^{-1} with a resolution of 0.12 cm^{-1}.

2.2. Computational Details. Calculations of stationary points and reaction profiles were first performed at a semiempirical level with the SAM1/d method[10] available in the Ampac 7.0 package.[11] The SAM1/d method was selected since chlorine and silicon d orbitals are taken into account. All stationary points (minima and transition states) were characterized by the calculation of the normal modes of the optimized structures. Reaction profiles were determined by a calculation with the CHAIN algorithm[12] and checked by the intrinsic reaction coordinate (IRC) method.

Semiempirical stationary points were the starting points of the density functional theory (DFT) calculations which were performed with the Gaussian 98 package.[13] All calculations were carried out at the B3PW91/6-31++G(d,p) level, and all stationary points were characterized by a calculation of the

* To whom correspondence should be addressed.
† Université de Provence.
‡ Université Paul Cézanne.

10.1021/jp044862o CCC: $30.25
Published on Web 02/15/2005

vibrational frequencies derived from the analytical second derivatives of the total energy of the optimized structures. Starting from the transition state (TS) structures, reaction profiles were determined by IRC calculations. The energy values were ZPE-corrected with vibrational frequencies scaled by 0.9772, as recommended by Scott and Radom.[14] The stabilization energy of the complexes involving **1** and **2** was corrected for basis set superposition error (BSSE) through the "7-point" formula taking into account monomer geometry relaxation.[15] For systems involving more than two subsystems in the reaction profiles, the electronic energy of the whole system was calculated by a single point with molecules 5 Å apart from each other. Only DFT calculations are reported in the next section.

3. Results and Discussions

To study the complexation between **1** and HCl, we have prepared at room temperature a gas mixture of these molecules. The infrared spectrum obtained after deposition on the cooled cell, shows the absorption band of acetyl chloride (**5**) and trimethylsilyl chloride (**4**). These results suggest that **1** reacts with HCl at room temperature in the gas phase as illustrated in Scheme 1. To determine the reaction mechanism and trap the van der Waals complex and the reaction intermediate **2**, argon matrixes were prepared by simultaneous spraying of separate mixtures of **1**/Ar and HCl/Ar at different concentrations and warming between 10 and 190 K. For comparison with the results obtained from the reaction between **1** and HCl, argon matrixes containing only **2**, **4**, or **5**, with different HCl concentrations were prepared and analyzed.

3.1. Infrared Absorption Spectra of 1/HCl/Ar. (A) Experimental Results. Infrared spectrum of monomer **1** is shown in Figure 1a, and the vibrational band[16] frequencies with their corresponding intensities are reported in Table 1. The most intense band, observed at 2120.5 cm^{-1}, is assigned to the ν_{CCOas}, whereas other small bands located around this value can be attributed to argon matrix effects.[17]

The spectrum recorded at 10 K after co-deposition of **1**/Ar (1/250) and HCl/Ar (3/250) shows new absorption bands compared to the spectra of pure **1** and pure HCl[18] trapped in an argon matrix (Figure 1b, Table 1). In the presence of HCl, the ν_{CCOas} band of **1** appears at 2109.5 cm^{-1}, shifted toward lower frequencies by 11 cm^{-1} with respect to the ν_{CCOas} band of monomer **1**. In the HCl region, we observe a band at 2600.7 cm^{-1} strongly shifted to lower frequencies ($\Delta\nu_{HCl}$ = 270.9 cm^{-1}). This important shift for ν_{HCl} is characteristic of a complexation between ketene derivatives and HCl.[1] Slightly shifted peaks are observed in the various spectral regions in which **1** absorbs (Figure 1a−c). All of these bands are indicative of the occurrence of a complex between **1** and HCl. The most distinct features of the complex are marked with an asterix in Figure 1. Different experiments, carried out with different concentration ratios, support the assignment of the complex bands (Table 1).

(B) Ab Initio Calculation Results. To model the complex structure, DFT calculations were carried out on several starting geometries. According to partial charges[19] and resonance structures of ketenes,[1,4,20] two geometric arrangements are possible for the **1**:HCl complex: the **L** form which involves a hydrogen bond between HCl and the oxygen atom of the ketene, and the **T** form, in which the HCl molecule interacts with the terminal carbon atom of the ketene. The optimized structures, reported in Scheme 2, show that in the **L** form the C═O bond is lengthened by 0.011 Å, while in the **T** form the C═C bond is lengthened by 0.008 Å (the HCl molecule is in the plane of the C═C π bond but is rather bound to C_3). The negative charge calculated with the ChelpG method[16] on the carbon atom C_3 of

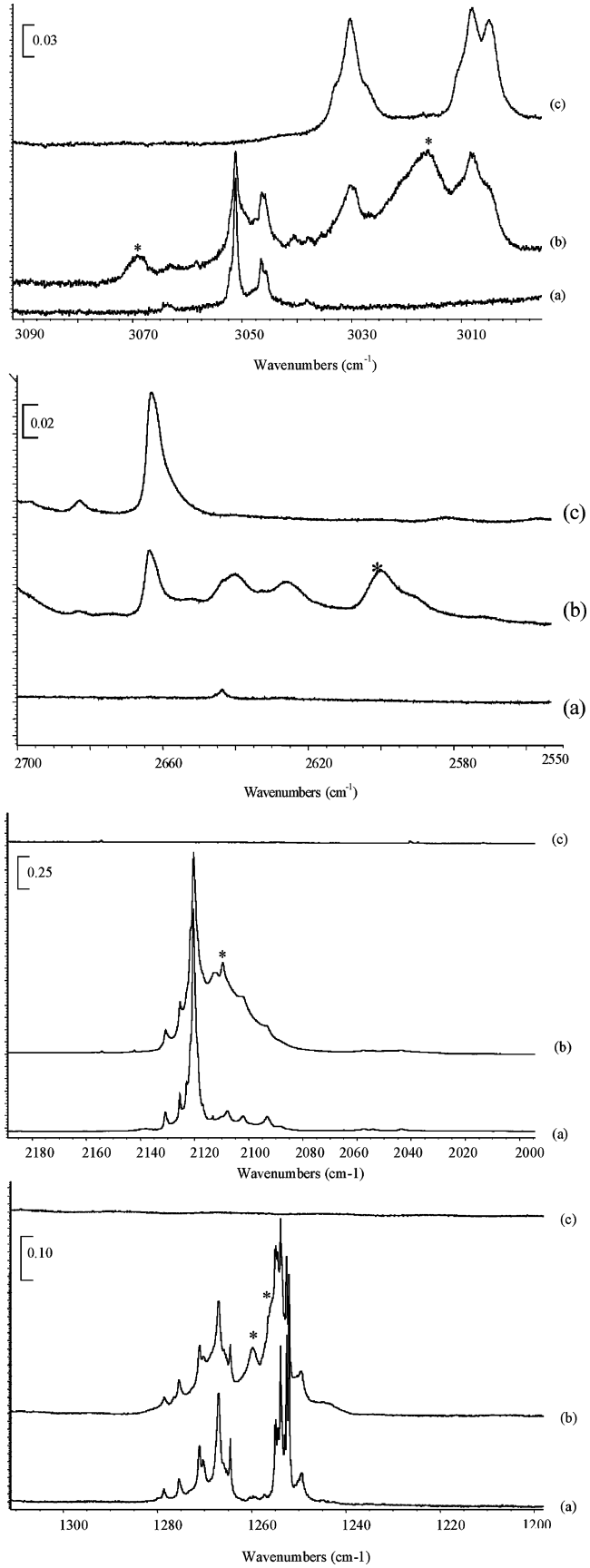

Figure 1. Infrared spectra of **1**, HCl and the **1**/HCl complex isolated in argon matrixes at 10 K in the 4000−1200 cm^{-1} region (a) **1**/Ar:1/500, (b) **1**/HCl/Ar:1/10/250 (c) HCl/Ar:10/500.

TABLE 1: Experimental and Theoretical Frequencies, and Frequency Shifts for 1 and 1:HCl Complexes[a]

	calculations								experiment		
	monomer		T complex			L complex			monomer	complex	
assignment	ν	int	ν	int	$\Delta\nu$	ν	int	$\Delta\nu$	ν	ν	$\Delta\nu$
					Silylketene **1**						
νH−C(CO)	3206	1	3191	1.6	*15*	3208	1.3	*−2*	3051.4	3069	−17.6
										3016.5	34.9
	3140	1.6	3149	0.5	*−9*	3143	0.9	*−3*			
	3140	1.6	3143	0.6	*−3*	3142	1.1	*−2*			
νCH(CH_3)	3139	0.01	3140	1.0	*−1*	3141	0.1	*−2*	2973.0		
	3136	1.2	3135	1.8	*1*	3136	1.0	*0*			
	3132	2.1	3133	0.8	*−1*	3134	1.2	*−2*			
	3129	0.01	3132	0.6	*−3*	3132	1.7	*−3*			
	3049	0.5	3050	0.3	*−1*	3050	0.2	*−1*			
νCH(CH_3)	3046	1	3049	0.7	*0*	3048	0.6	*−2*	2913.3		
	3045	0.85	3046	0.6	*−1*	3047	0.5	*−2*			
νas(C)CO	2209	100	2203	100	*6*	2192	100	*17*	2120.5	2109.5	11
	1475	0.97	1475	1	*0*	1474	0.8	*1*			
	1469	0.82	1467	0.9	*2*	1469	0.7	*0*			
δasCH_3	1465	0.5	1466	0.5	*−1*	1465	0.4	*0*	1417.0		
	1457	0.01	1456	0.06	*1*	1456	0.03	*1*			
	1456	0.01	1455	0.02	*1*	1455	0.03	*1*			
	1451	0.	1452	0.02	*−1*	1452	30.0	*−1*			
νsCC(O)	1319	5.3	1308	1.4	*11*	1319	2.6	*0*	1267.0	1259.8	7.2
	1303	1.3	1300	8.2	*3*	1304	0.9	*−1*			
δsCH_3	1292	3.6	1296	2.0	*−4*	1294	3.0	*−2*	1252.8	1256.0	−3.2
	1288	4.3	1291	4.0	*−3*	1290	5.5	*−2*			
δH−C(CO)	1059	4.7	1060	3.9	*−1*	1050	5.5	*9*	1046.6		
	885	18.6	882	4.1	*3*	883	15.5	*2*			
ρCH_3	874	9.5	880	16.9	*6*	877	7.7	*−3*	852.0		
	871	9	876	10.1	*−5*	872	7.3	*−1*			
νasSiC_3 or $Si(CH_3)_3$	797	1.7	798	8.7	*−1*	797	1.4	*0*	777.0		
$Si(CH_3)_3$	777	3.4	778	1.8	*−1*	779	2.6	*−2*	758.0		
					HCl						
	2897	100	2534	98	453	2846	43	141	2871.0	2600.7	270.9

[a] $\Delta\nu = \nu_{complex} - \nu_{monomer}$.

SCHEME 2: Optimized Geometries at the B3PW91/6-31++G(d,p) Level of 1 and 1:HCl Complexes. Interatomic Distances Are Given in Angströms and Angles in Degrees. Relative Energies Are BSSE-corrected

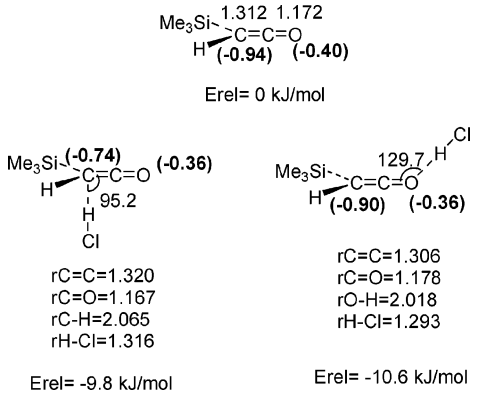

ketene **1** is more important (−0.94) than on the oxygen atom (−0.40). It is important to note that the presence of a silicon atom on the C_3 carbon atom modifies the charge on this atom with respect to the parent ketene H_2C_2O,[18] but that the terminal oxygen charge is unchanged. This carbon atom can be considered as a good site of reactivity for electrophiles.

We have considered the relative energies of the two complexes (Scheme 2, Table S1 in the Supporting Information): the **L** form is more stable than the **T** form by less than 1 kJ mol^{-1}. This difference is not significant enough to identify unambiguously the structure observed in the matrix. Indeed, use of MP2 procedure with the 6-31++G (d,p) basis set shows a greater stability of the **T** complex (4.8 kJ/mol).

To try to identify the form present in our experiment, we must compare the vibrational frequency shifts of the two complexes with regard to the calculated ones for the free molecule. The experimental and the calculated shifts are in good agreement and confirm the complexation between the two molecules but we cannot conclude about the complex structure (Table 1).

3.2. Annealing Experiments. (A) Experimental Results. Warm up of the matrix previously obtained, containing **1**, HCl, and **1**:HCl complex, to 40 K, induces changes in the IR spectra: the absorption bands of **1**, HCl, and **1**:HCl complex start to decrease and new small absorption bands appear in different areas of the spectrum.

Above 45 K, argon sublimes and the infrared spectrum of a solid sample containing essentially **1** and HCl is observed. During the annealing, these two compounds react (their absorption bands decrease) and we observe the increase of different absorption bands. The most interesting spectra area, showed in Figure 2, is characteristic of the stretching mode $\nu_{C=O}$. In this area, during the annealing, four absorption bands at 1784, 1765, 1739, and 1703 cm^{-1} appear. These bands were attributed to intermediate **2**. To verify this hypothesis compound **2** has been synthesized and trapped in argon matrix. Likewise, we have isolated in argon matrix **5** and **4** monomer molecules. Comparison between these spectra and the ones of our previous experiments (Figure 3) allowed the assignment of bands observed at 1784 and 1765 cm^{-1} to **2**. Also, the most intense band of acetyl chloride monomer at 1807 cm^{-1} is not observed in our experiment.

The bands observed at 1703 and 1739 cm^{-1}, shifted to lower frequencies with respect to the vibrational bands of the

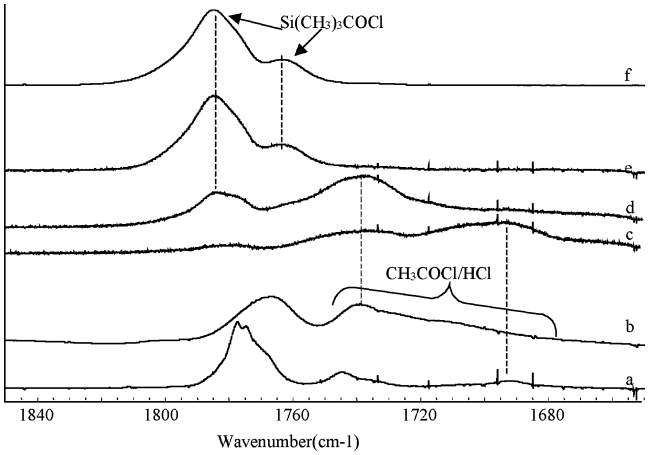

Figure 2. Infrared spectra of the different reaction products in ν_{CO} range. (a) MeCOCl/HC/Ar:1/40/500, T_s = 40 K, (b) MeCOCl/HCl/Ar:1/40/500, T_s = 80 K, (c) **1**/HCl/Ar:1/3/500, T_s = 70 K, (d) **1**/HCl/Ar:1/3/500, T_s = 80 K, (e) **1**/HCl/Ar:1/3/500 T_s = 120 K, (f): **2**/Ar:1/500, T_s = 120 K.

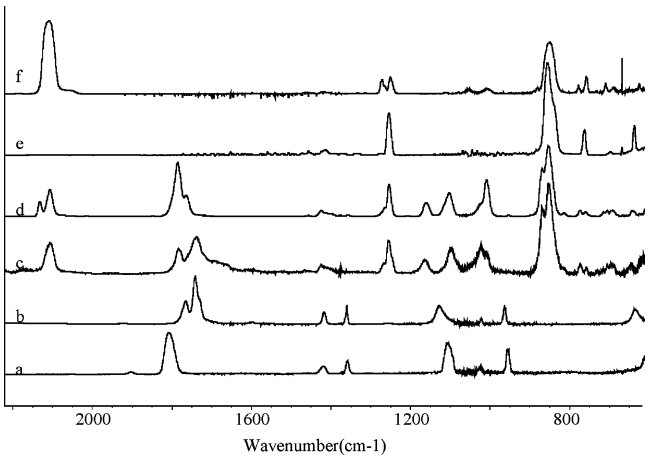

Figure 3. Infrared spectra at 80 K of the different reaction products. (a) MeCOCl/Ar:1/500, (b) MeCOCl/HCl/Ar:1/40/500, (c) **1**/HCl/Ar:1/3/500, (d) **2**/HCl:1/500, (e) Me_3SiCl/Ar:1/500, (f) **1**/Ar:1/500.

monomer, are characteristic of a complexed carbonyl group.[21] To identify this complex, we have performed argon matrix experiments with acetyl chloride/HCl mixture at different concentrations. The spectra recorded at 10 K after deposition of CH_3COCl/HCl/Ar (1/13/500, 1/40/500) show new absorption bands (Figure 4, Table 2) with respect to those of pure CH_3COCl and HCl trapped in argon matrix. These bands are attributed to complexes between CH_3COCl and HCl. In the ν_{CO} stretching region of acetyl chloride (Figure 4a), we observed two bands at 1777.4 and 1743.0 cm^{-1}, shifted toward lower frequencies by 33.9 and 68.3 cm^{-1} with regard to the absorption band of the monomer (1811.3 cm^{-1}). In the ν_{HCl} region, three bands appear (Figure 4B) at 2724.2, 2675.3, and 2632.3 cm^{-1}, shifted to lower frequencies by 145.8, 194.7, and 237.7 cm^{-1} with respect to the HCl monomer absorption band (2870.0 cm^{-1}). For the 1/40/500 mixture, we observe in the ν_{CO} area a supplementary band at 1695.0 cm^{-1} attributed to the ν_{CO} stretching of acetyl chloride complexed by several HCl molecules. At this concentration, the HCl bands are saturated and are not presented in Figure 4B.

The structure and vibrational frequencies of 1:1 and 1:2 acetyl chloride/HCl complexes were calculated. As a large $\nu_{C=O}$ shift is observed, only two 1:1 (**5a**, **5b**) and two 1:2 (**5c**, **5d**) arrangements, complexed on the oxygen atom, were investigated (Scheme 3). The comparison between the experimental and

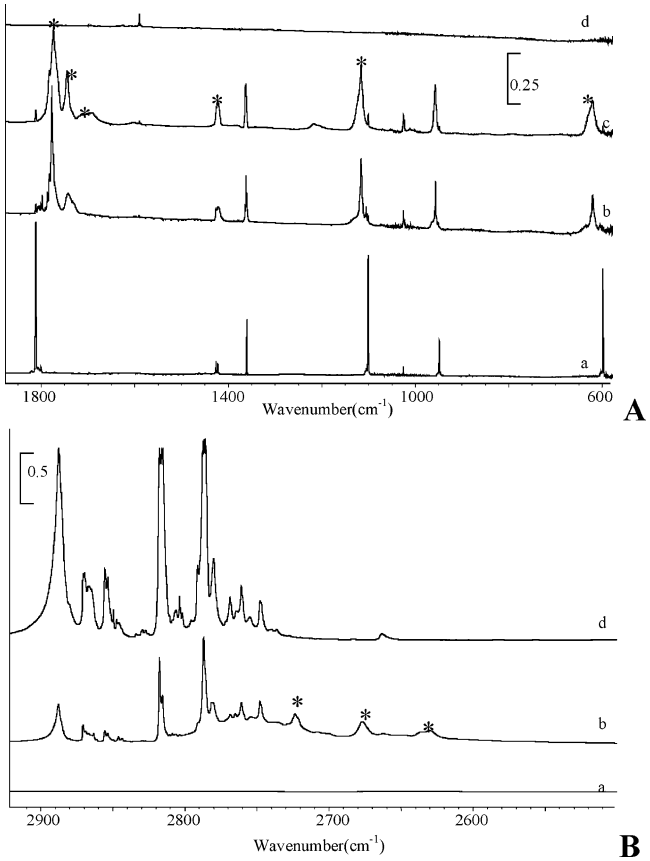

Figure 4. Infrared spectra of the CH_3COCl/HCl complexes isolated in argon matrix at 10 K in different regions. [(A) CH_3COCl region, (B)] HCl region. (a) CH_3COCl/Ar:1/500, (b) CH_3COCl/HCl/Ar:1/13/500, (c) CH_3COCl/HCl/Ar:1/40/500, (d) HCl/Ar:1/500. the bands noted by an asterix are attributed to the MeCOCl/HCl complex.

theoretical frequency shifts, summarized in Table 2, shows a good agreement with both 1:1 complex structures and the 1:2 complex structure **5d**. Thus, in the annealing experiments (Figure 2), the bands at 1703 and 1739 cm^{-1} are attributed to a 1:*n* complex ($n > 2$) and a 1:2 complex, respectively.

Then, during the annealing **2**, **4**, and **5**:HCl complexes are formed. Nevertheless, Figure 2 shows that the bands at 1739 and 1703 cm^{-1} appear from 50 K (Figure 2c). Above 70 K the $CH_3COCl:(HCl)_n$ band observed at 1703 cm^{-1} disappears, whereas the $CH_3COCl:(HCl)_2$ absorption band at 1739 cm^{-1} increases until 80 K (Figure 2d). Above this temperature, this band decreases. The two absorption bands at 1784 cm^{-1} and at 1765 cm^{-1}, which appear from 80 K, increase until 120 K, a temperature above which the product starts to desorb (Figure 2c). The same annealing experiments were performed for the different concentrations. Figure 5 shows the results obtained at 70 K in the $\nu_{C=O}$ region. We note that the 1703 cm^{-1} band is more intense for large HCl concentrations (1/10/500). This band is not present for the 1/1/500 concentration, whereas we observed the band at 1739 and 1784 cm^{-1}. For the 3/1/500 concentration only the band at 1784 cm^{-1} is observed. This comparison shows that the observation of **2** is HCl concentration dependent.

From all of these experiments, we can say that during the annealing **1** reacts with HCl molecules (many being present in the medium) to yield **5**:$(HCl)_n$, **5**:$(HCl)_2$, and **4**. Then, we oberve a regular decrease of HCl absorption until its total desorption at about 90 K. Above this temperature the **5**:$(HCl)_n$ complex absorption bands disappear and the **5**:$(HCl)_2$ ones increase. We observe intermediate ***2*** only between 70 and 80 K. Above this

TABLE 2: Experimental and Theoretical Frequencies, and Frequency Shifts for Acetyl Chloride and Acetyl Chloride:HCl Complexes[a]

	calculations								experiment				
		complex **5a**		complex **5b**		complex **5c**		complex **5d**		complex			attribution
	monomer	ν	$\Delta\nu$	ν	$\Delta\nu$	ν	$\Delta\nu$	ν	$\Delta\nu$	monomer	ν^a	ν^b	$\Delta\nu$	CH_3COCl:HCl complexes
CH_3COCl	3189	3188	−1	3192	3	3190	1	3188	−1					
	3158	3155	−3	3156	−2	3154	−4	3154	−4	3028				
	3074	3073	−1	3073	−1	3072	−2	3072	−2					
	1901	1858	**−43**	1863	**−38**	1825	**−76**	1851	**−50**	1811.3	1777.4	1777.4	**−33.9**	1:1
											1743.0	1743.0	**−68.3**	1:2
												1695.0	**−116.3**	1:n
	1466	1464	−2	1464	−2	1463	−3	1464	−2	1426.1				
	1462	1462	0	1461	−1	1461	−1	1463	1	1422.5				
	1392	1393	1	1394	2	1394	2	1395	3	1360	1363.4/1361.8	1363.4/1361.8	3.4/1.8	
	1121	1135	14	1131	10	1145	24	1135	14	1100.2	1115.8/1112.2	1115.8/1112.2	15.2/12.	
	1041	1041	0	1040	−1	1041	0	1041	0	1025.1				
	969	974	5	976	7	979	10	974	5	948.7	956.0/954.1/ 953.0	956.0/954.1/ 953.0	7.3/5.4/4.3	
	615	638	23	634	19	654	39	638	23	598.4	625.4/619.3	625.4/619.3	27.0/20.9	
HCl	2987	2789	**−198**	2829	**−158**	2857	**−130**	2803	**−184**	2870	2724.2		**−145.8**	1:1
						2830	**−157**	2734	**−253**		2675.3		**−194.7**	1:2
											2632.3		**−237.7**	1:2

[a] $\Delta\nu = \nu_{complex} - \nu_{monomer}$. [b] 1/13/500. [c] 1/40/500.

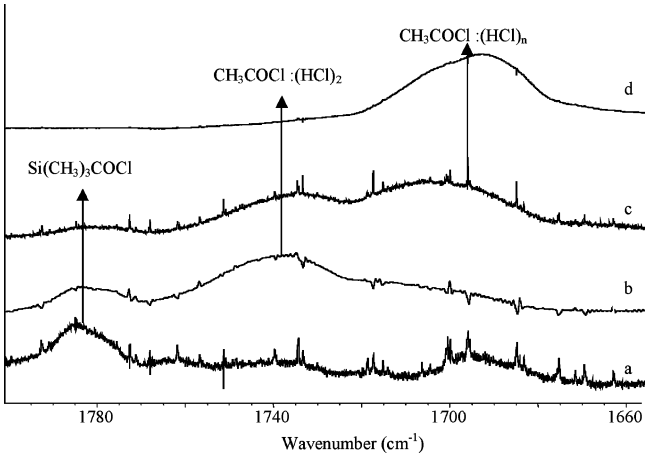

Figure 5. Infrared spectra of product from annealing at 70 K of **1**/HCl/Ar mixture (a) 3/1/500, (b)1/1/500, (c)1/3/500, (d)1/10/500.

SCHEME 3: Arrangements of 5:HCl and 5:$(HCl)_2$ Complexes and Their Energies in Hartree

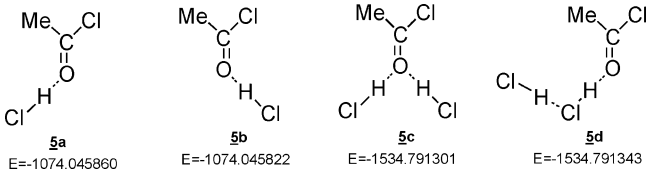

temperature the amount of HCl is not sufficient in the medium to form complexed or monomer acetyl chloride. The reaction is stopped after the addition of the first HCl molecule and we observe only intermediate **2**.

(B) Ab Initio Calculation Results. Starting from both **L** and **T 1**:HCl complexes, we investigated various reaction mechanisms.

Reaction Profile Starting from the T Form Complex. A reaction profile involving three steps and three main complexes is proposed; the transition state strutures are given in Figure 6, and the optimized structures of the main minima in Figure S1 in the Supporting Information. Experimental vibrational spectra showed that final products formed van der Waals complexes with at least two HCl molecules. To be in agreement with this

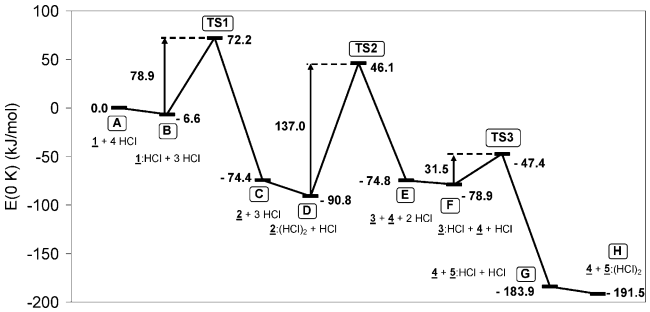

Figure 6. Reaction profile I. **3**: $CH_2C(OH)Cl$.

experimental observation, four HCl molecules were involved in the whole process. After the complexation between an HCl molecule and the carbon atom C_3 of **1**, the intermediate structure **2** was obtained through the asynchronous concerted addition of HCl to the $C_2{=}C_3$ double bond with an activation energy of 78.9 kJ mol^{-1} (Figure 6, Table S2 in the Supporting Information). This first activation energy is consistent with the experimental observation of the addition occurring from 40 K. The formation of a complex between the oxygen atom of **2** and two HCl molecules stabilized the system by 16.4 kJ mol^{-1} (Figure 6). The **2**:$(HCl)_2$ complex evolved by a dissociative process (cleavage of the Si−C bond) to give enol chloride **3** ($CH_2{=}C(OH)Cl$) and trimethylsilyl chloride **4** (formation of a Si−Cl bond). In this profile, two HCl molecules are involved in **TS2** but a similar activation energy was obtained (137.0 kJ mol^{-1}) with only one HCl molecule. **TS2** is lower in energy than **TS1** because a pseudo six-membered ring is formed (Figure 7). Moreover, the reaction occurs with retention of configuration on the silicon atom which is in agreement with previous studies on the 1,3-silyl shift.[22] In the transiton state of this retention path, the Si atom is pyramidal and forms a partial Si−C bond (2.55 Å) and a partial Si−Cl bond (2.52 Å) between its vacant d orbital, and the p orbital of C_3 and the lone pair of the Cl atom, respectively. Enol chloride **3** might also form a complex (**3**:HCl) with another HCl molecule. In agreement with the partial charges and coefficients of the LUMO, the HCl molecule is bound to carbon atom C_3. The last step then required a small activation energy (31.5 kJ mol^{-1}) to give the final products, **4**

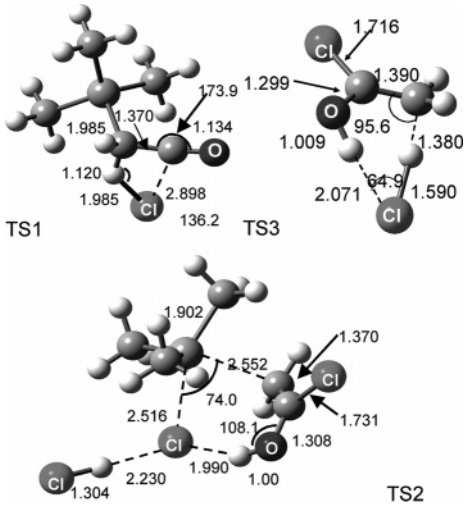

Figure 7. Structure of the transition states of reaction profile I. Interatomic distances are given in angströms and angles in degrees.

and **5**:$(HCl)_2$. The last step was again particularly favored since a pseudo six-membered ring was formed in **TS3** structure (Figure 7).

Alternative routes to this reaction path were also investigated. First, a direct addition of the HCl molecule of **2**:HCl and the following cleavage of the Si−C bond were considered. This approach directly gives **4** and **5**, with an activation energy of 212.4 kJ mol^{-1} (electronic energy). However, this reaction profile was not in agreement with experimental observations because: (i) the activation energy of the second step was too high to explain the detection of **4** and **5** from 50 K; (ii) the intermediate trimethylacetyl chloride **2** should have been detected before the final products.

In a second hypothesis, the activation energy of a last step involving an intramolecular keto−enolic conversion starting from **3** was again too large (211.2 vs 31.5 kJ mol^{-1}) to be consistent with experimental observations (Figure 6).

The whole reaction profile I was thus consistent with experimental data. As soon as enough energy is provided to the system to reach the first transition state structure (**TS1**), and since all the following stationary points are lower in energy, the total reaction sequence takes place and the final products are detected. When HCl molecules desorb, due to annealing, the reaction is stopped at the **2**:HCl complex and **5**:HCl complexes are not formed because of the lack of HCl molecules.

Reaction Profiles Starting from the L Form Complex. As experimental IR bands might be attributed to the **T** form or **L** form of **1**:HCl, we considered an alternative route starting from the **L** form (reaction profile II, Figures S2 and S3 in the Supporting Information). With a first addition of HCl to the C_2═O double bond, silylenolchloride **6** ($SiMe_3CHC(OH)Cl$) is obtained via transition state **TS1′**. The activation energy for this first step is 157.1 kJ mol^{-1}, i.e., two times higher than for addition to the C_2═C_3 double bond starting from the **T** form (profile I), and moreover the step is endothermic. Consequently, this mechanism was not considered further. Nevertheless, a second reaction profile starting from the **L** form of **1**:HCl and involving a second HCl molecule, to reduce the hindrance in **TS1′**, was investigated (reaction profile III, Figure 8). The resulting transition state **TS1″** is only 12 kJ mol^{-1} higher in energy than **TS1** since a pseudo six-membered ring is formed. The first step is slightly endothermic but the second step leading to compound **2**:$(HCl)_2$ only requires 25.1 kJ mol^{-1} and is highly exothermic. Hence, it may be a competitive pathway. The

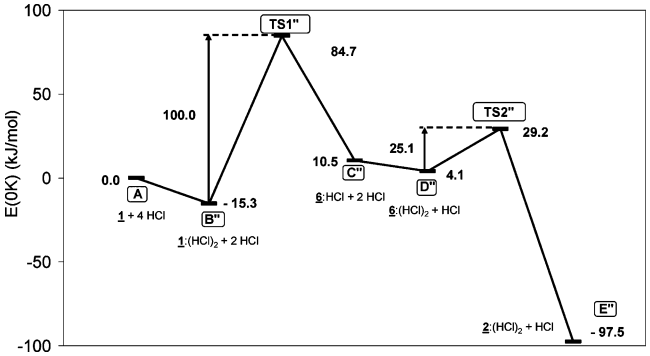

Figure 8. First steps of reaction profile III. **6**: $SiMe_3CHC(OH)Cl$.

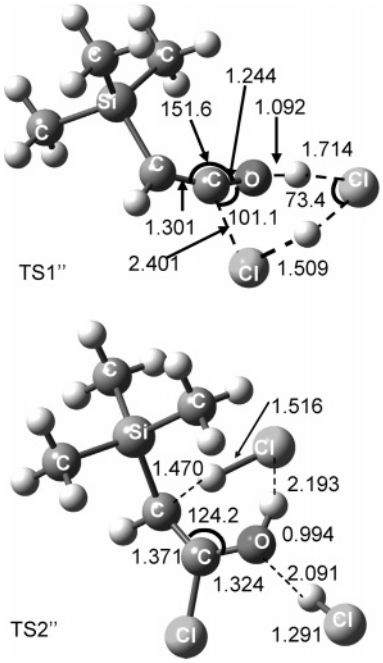

Figure 9. Structure of transition states **TS1″** and **TS2″** of reaction profile III. Interatomic distances are given in angströms and angles in degrees.

structure of transition states of reaction profile III are given in Figure 9 and the structure of the main minima in Figure S4 in the Supporting Information.

4. Conclusion

In this paper, we have first established, by means of FTIR argon matrix experiments, that the reaction between **1** and hydrogen chloride (HCl) at room and low-temperature involves a cleavage of the Si−C bond and leads to trimethylsilyl chloride and acetyl chloride/HCl complexes. A DFT study led us to propose a multistep profile accounting for the reaction and involving, as an intermediate, trimethylsilylacetyl chloride. The occurrence of such an intermediate was confirmed by experiments carried out under low concentration of HCl. This work brings another example of the particular reactivity of silylketenes among the ketene family.

Acknowledgment. The authors gratefully acknowledge the "Institut du Développement et des Ressources en Informatique Scientifique" (IDRIS) and the "Centre de Ressources Informatiques de Haute Normandie" (CRIHAN) for grants of computer time and L. Fournier for providing trimethylsilylketene and trimethylsilylacetyl chloride. This work was also supported by the computing facilities of the CRC-MM, "Centre Régional de Compétences en Modélisation Moléculaire de Marseille, France".

Supporting Information Available: Table S1 showing relative stability and structural parameters of **1**:HCl complexes calculated at the B3PW91/6-31+G(d,p) level (1 page). Table S2 giving energy data, from DFT calculations at the B3PW91/6-31++G(d,p), for all compounds of profile I, II et III. Figure S1 showing the optimized structures of the main minima of reaction profile I. Figure S2 showing reaction profile II. Figure S3 showing the optimized structure of the transition state **TS1′** and the main minima of reaction profile II. Figure S4 showing the optimized strutures of the main minima of reaction profile III. This material is available free of charge via the Internet at http://pubs.acs.org.

References and Notes

(1) (a) Tidwell, T. T.; Ketenes, J. Wiley & Sons Ed.: New York, 1995. (b) Soper, P. D.; Legon, A. C.; Flygare, W. H. *J. Chem. Phys*. **1981**, *74*, 2138. (c) Barnes, A. J.; Lasson, E.; Nielson, C. J. *J. Chem. Soc., Faraday Trans* **1995**, *91*, 3111. (d) Kogure, N.; Hatakeyama, R.; Suzuki, E.; Watari, F. J. *J. Mol. Struct*. **1993**, *299*, 105.

(2) (a) Lundell, J.; Räsänen, M. *J. Phys. Chem*. **1995**, *99*, 14301. (b) Sadleg, J.; Roos, B. O. *Theor. Chim. Acta* **1989**, *73*, 173.

(3) Piétri, N.; Chiavassa, T.; Allouche, A.; Aycard, J. P. *J. Phys. Chem. A* **1997**, *101*, 1093.

(4) Schukovskaya, L. L.; Palchick, R. I.; Lazarev, A. N. *Dokl. Akad. Nauk. S.S.S.R.* **1965**, *164*, 357 (Chem. Abst. **1965**, *63*, 18138g).

(5) Allen, A. D.; Tidwell, T. T. *Tetrahedron Lett*. **1991**, *32*, 847.

(6) (a) Colvin, E. W. *Silicon in Organic Synthesis*; Butterworths: London, 1981; p 174. (b) ref 1 p348. (c) Pommier, A.; Kocienki, P.; Pons, J. M. *J. Chem. Soc., Perkin Trans. 1* **1998**, 2105. (d) Shiori, T.; Takaoka, K.; Aoyama, T. *J. Heterocycl. Chem*. **1999**, *36*, 1555. (e) Pons, J. M.; Kocienski, P. *Science of Synthesis*; Flenning, I., Ed.; Thieme: Stuttgart, Germany, 2002; Vol 4, p 657.

(7) (a) Pommier, A.; Pons, J. M.; Kocienski, P. J.; Wong, L. *Synthesis* **1994**, 1294. (b) Pommier, A.; Pons, J. M.; Kocienski, P. J. *J. Org. Chem*. **1995**, *60*, 7334. (c) Kocienski, P. J.; Pelotier, B.; Pons, J. M.; Prideaux, H. *J. Chem. Soc., Perkin Trans. 1* **1998**, 1373. (d) Dymock, B. W.; Kocienski, P. J.; Pons. J. M. *Synthesis* **1998**, 1655.

(8) (a) Molina. P.; Vidal, A.; Barquero, I. *Synthesis* **1996**, 1199. (b) Molina, P.; Vidal, A.; Tovar, F. *Synthesis* **1997**, 963.

(9) Kostyuk, A. S.; Boyadzhau, Z. G.; Zaitseva, G. S.; Sergeev, V. N.; Savel'eva, N. I.; Baukov, Y. I.; Lutseuko, I. F. *J. Gen. Chem. U.S.S.R. (Engl. Trans.)* **1979**, *49*, 1346.

(10) Dewar, M. J. S.; Jie, C.; Yu, J. *Tetrahedron* **1993**, *49*, 5003−5038.

(11) Ampac 7.0, Semichem Inc. PO Box 1649, Shawnee Mission, KS 66222, 2001.

(12) Liotard, D. A. *Int. J. Quantum Chem.* **1992**, *44*, 723.

(13) Frisch, M. J.; Trucks, G. W.; Schlegel, H. B.; Scuseria, G. E.; Robb, M. A.; Cheeseman, J. R.; Zakrzewski, V. G.; Montgomery, J. A., Jr.; Stratmann, R. E.; Burant, J. C.; Dapprich, S.; Millam, J. M.; Daniels, A. D.; Kudin, K. N.; Strain, M. C.; Farkas, O.; Tomasi, J.; Barone, V.; Cossi, M.; Cammi, R.; Mennucci, B.; Pomelli, C.; Adamo, C.; Clifford, S.; Ochterski, J.; Petersson, G. A.; Ayala, P. Y.; Cui, Q.; Morokuma, K.; Malick, D. K.; Rabuck, A. D.; Raghavachari, K.; Foresman, J. B.; Cioslowski, J.; Ortiz, J. V.; Stefanov, B. B.; Liu, G.; Liashenko, A.; Piskorz, P.; Komaromi, I.; Gomperts, R.; Martin, R. L.; Fox, D. J.; Keith, T.; Al-Laham, M. A.; Peng, C. Y.; Nanayakkara, A.; Gonzalez, C.; Challacombe, M.; Gill, P. M. W.; Johnson, B. G.; Chen, W.; Wong, M. W.; Andres, J. L.; Head-Gordon, M.; Replogle, E. S.; Pople, J. A. *Gaussian 98*, revision A.11.4; Gaussian, Inc.: Pittsburgh, PA, 1998.

(14) Scott, A. P.; Radom, L. *J. Phys. Chem.* **1996**, *100*, 16502.

(15) (a) Boys, S. F.; Bernardi, F. *Mol. Phys.* **1970**, *19*, 553. (b) Lendvay, G.; Mayer, I. *Chem. Phys. Lett.* **1998**, *297*, 365.

(16) Lazarev, A. N.; Tenisheva, T. F.; Shchukovskaya, L. L. *Zh. Fiz. Khim*. **1969**, *43*, 1692.

(17) Jacox, M. E.; Milligan, D. E. *J. Chem. Phys*. **1965**, *43*, 3734.

(18) (a) Barnes, A. J.; Hallam, H. E.; Scrimshaw, G. F. *Trans. Faraday. Soc*. **1969**, *86*, 3150. (b) Perchard, J. P.; Cipriani, J.; Silvi, B.; Maillard, D. *J. Mol. Struct*. **1983**, *100*, 317. (c) Maillard, D.; Schriver, A.; Perchard, J. P. *J. Chem. Phys*. **1979**, *71*, 505.

(19) Breneman, C. M.; Wiberg, K. B. *J. Comput. Chem.* **1990**, *11*, 361.

(20) (a) Gong, L.; McAllister, M. A.; Tidwell, T. T. *J. Am. Chem. Soc.* **1991**, *113*, 6027.

(21) (a) Dudis, D. S.; Everhart, J. B.; Branch, T. M.; Hunnicutt, S. S. *J. Phys. Chem*. **1996**, *100*, 2083. (b) Schriver, L. *J. Chem. Soc., Faraday. Trans. 2* **1989**, *85*, 607.

(22) (a) Oblin, M.; Fotiadu, F.; Rajzmann, M.; Pons, J.-M. *J. Chem. Soc., Perkin Trans. 2* **1997**, 1621. (b) Yamabe, T.; Nakamura, K.; Shiota, Y.; Yoshizawa, K.; Kawauchi, S.; Ishikawa, M. *J. Am. Chem. Soc.* **1997**, *119*, 807. (c) Ohshita, J.; Niwa, H.; Ishikawa, M.; Yamabe, T.; Yoshii, T.; Nakamura, K. *J. Am. Chem. Soc.* **1996**, *118*, 6853. (d) Antoniotti, P.; Canepa, C.; Tonachini, G. *J. Org. Chem.* **1994**, *59*, 3952. (e) Takahashi, M.; Kira, M. *Proc. Symp. Organomet. Chem. Jpn., 10th* **1993**, 205.